ELSEVIER

Catalysis Today 59 (2000) 347–363

CATALYSIS TODAY

www.elsevier.com/locate/cattod

# Catalytic behavior of La–Sr–Ce–Fe–O mixed oxidic/perovskitic systems for the NO+CO and NO+$CH_4$+$O_2$ (lean-$NO_x$) reactions

V.C. Belessi[a], C.N. Costa[b], T.V. Bakas[c], T. Anastasiadou[b], P.J. Pomonis[a,*], A.M. Efstathiou[b,1]

[a] *Department of Chemistry, University of Ioannina, Ioannina 45110, Greece*
[b] *Department of Chemistry, University of Cyprus, PO Box 20537, CY 1678 Nicosia, Cyprus*
[c] *Department of Physics, University of Ioannina, Ioannina 45110, Greece*

**Abstract**

Mixed oxides of the general formula $La_{0.5}Sr_xCe_yFeO_z$ were prepared by using the nitrate method and characterized by XRD and Mössbauer techniques. The crystal phases detected were perovskites $LaFeO_3$ and $SrFeO_{3-x}$ and oxides α-$Fe_2O_3$ and $CeO_2$ depending on *x* and *y* values. The low surface area ceramic materials have been tested for the NO+CO and NO+$CH_4$+$O_2$ ("lean-$NO_x$") reactions in the temperature range 250–550°C. A noticeable enhancement in NO conversion was achieved by the substitution of $La^{3+}$ cation at A-site with divalent $Sr^{+2}$ and tetravalent $Ce^{+4}$ cations. Comparison of the activity of the present and other perovskite-type materials has pointed out that the ability of the $La_{0.5}Sr_xCe_yFeO_z$ materials to reduce NO by CO or by $CH_4$ under "lean-$NO_x$" conditions is very satisfying. In particular, for the NO+CO reaction estimation of turnover frequencies (TOFs, $s^{-1}$) at 300°C (based on NO chemisorption) revealed values comparable to Rh/α-$Al_2O_3$ catalyst. This is an important result considering the current tendency for replacing the very active but expensive Rh and Pt metals. It was found that there is a direct correlation between the percentage of crystal phases containing iron in $La_{0.5}Sr_xCe_yFeO_z$ solids and their catalytic activity. $O_2$ TPD (temperature-programmed desorption) and NO TPD studies confirmed that the catalytic activity for both tested reactions is related to the defect positions in the lattice of the catalysts (e.g., oxygen vacancies, cationic defects). Additionally, a remarkable oscillatory behavior during $O_2$ TPD studies was observed for the $La_{0.5}Sr_{0.2}Ce_{0.3}FeO_z$ and $La_{0.5}Sr_{0.5}FeO_z$ solids. 

*Keywords:* Perovskites; NO reduction; Lean-$NO_x$; $O_2$ TPD; NO TPD; Oscillations

## 1. Introduction

The development of new catalysts for the selective reduction of $NO_x$ emissions from both stationary and mobile sources has gained an increasing interest in the last few years. This is due to the need for replacing the $NH_3$-SCR process with possibly an HC-SCR process (hydrocarbon-selective catalytic reduction) and demands for improvement of fuel economy in internal combustion engines with low $CO_2$ emissions. The latter has pushed the car industry towards "lean-burn" engine technology and other strategies for automotive "lean-$NO_x$" emission control [1–5].

Noble metals (especially Pt) have proven to be promising components of a "lean-$NO_x$" catalyst with particular applications in diesel internal combustion engines (low-temperature $NO_x$ reduction in strongly

* Corresponding author. Fax: +30651-44836.
*E-mail addresses:* ppomonis@cc.uoi.gr (P.J. Pomonis), efstath@ucy.ac.cy (A.M. Efstathiou)
[1] Co-corresponding author. Fax:+3572-339060.

0920-5861/00/$ – see front matter 
PII: S0920-5861(00)00300-X

oxidizing conditions) and "lean-burn" engines as well [6,7]. However, their cost and availability make it reasonable to search for alternative materials. Perovskite-type oxides of the general formula $ABO_3$ have proven to be an important class of catalytic materials. The catalytic reduction of NO with CO [8–13], CO and $H_2$ [14], $H_2$ [15], hydrocarbons [16,17] and $NH_3$ [18] have been investigated over perovskites. There have also been attempts to combine the catalytic behavior of noble metals with that of perovskites [19,20]. However, most of the studies concerning the reaction of NO+CO have been carried out mainly on noble metals [21–23]. There is little work reported in the literature concerning "lean-$NO_x$" catalysis by using hydrocarbons as reducing agents over perovskite-type oxides [1,16,17,24,25], where propylene was the main reducing agent used.

The properties of perovskites $ABO_3$ can be easily modified by the substitution of the A cation, usually $La^{3+}$, by another cation of lower or higher oxidation state, e.g., $Sr^{2+}$ or $Ce^{4+}$. In this case, the charge compensation is achieved either by the formation of oxygen ion vacancies or by the formation of mixed oxidation states (e.g., $La_{1-x}{}^{3+}Sr_x{}^{2+}M_{1-x}{}^{3+}M_x{}^{4+}O_3$), or a combination of those two possibilities. In some cases, the formation of cationic vacancies can also take place. The high catalytic activity of such substituted structures is related to their defects and the effect of the valence alteration on the catalytic activity has been extensively studied [26–31]. However, there has been very little work reported in the literature about the effect on the catalytic activity of a double substitution in A-position which would theoretically lead to a triple oxidation state for the B cation.

The only work that examined such a double substitution in A-position has been referred to the system of $La_{1-x-y}Sr_xCe_yCoO_3$ [32] for the oxidation of HC and CO. Voorhoeve et al. [14] have also examined the $La_{0.85}Bi_{0.08}K_{0.07}MnO_3$ ($Bi^{+3}$ and $K^+$ were substituted for $La^{+3}$) system for its catalytic activity towards NO reduction by CO and $H_2$. High activity but poor stability (because of the presence of low melting point components) was reported and the presence of $Mn^{+3}/Mn^{+4}$ was mentioned.

In the present work, $Sr^{2+}$ and $Ce^{4+}$ have been substitutionally added instead of $La^{3+}$ in the $LaFeO_3$ solid in varying atomic ratios in order to alter the oxidation state of Fe and the concentration of oxygen vacancies in the original perovskite material. The solids thus obtained have been investigated for two environmentally important catalytic reactions, the NO+CO and the $CH_4$+NO+$O_2$ ("lean-$NO_x$") reactions. The structure of the solids was examined by XRD and the precise determination of the amount of crystal phases of each of the solids containing iron was determined by Mössbauer spectroscopy. Transient experiments were conducted in order to study the interaction of molecular species of interest with the catalyst surface. The information obtained from catalyst characterization and transient studies was correlated with the catalytic performance of the materials.

## 2. Experimental

### 2.1. Preparation of materials

The materials $La_{1-x-y}Sr_xCe_yFeO_3$ for various values of *x* and *y* were prepared using the nitrate method as follows: calculated amounts of $La(NO_3)_3{\cdot}6H_2O$ (Merck), $Fe(NO_3)_3{\cdot}9H_2O$ (Merck), $Sr(NO_3)_2$ (Ferak) and $CeO_2$ (Aldrich) were mixed thoroughly in an agate mortar and heated slowly up to 400°C for nitrate decomposition. At the end of this step (no visible $NO_2$ fumes), the system was further heated for 4 h at 900°C at 1 atm. Then, the mixture was removed from the furnace, cooled and after grinding was heated again for another 4 h at 1050°C. The sample was then slowly cooled to room temperature and stored for further use. It is mentioned that the notation $La_{1-x-y}Sr_xCe_yFeO_3$ will be employed indicating just the nominal composition of the solids. This has nothing to do with particular crystal phases existing in each sample.

### 2.2. Characterization of materials

*XRD analysis*. The crystal structure of the prepared materials was determined by XRD analysis using a SIEMENS Diffract 500 system employing Cu Kα radiation (λ=1.5418 Å).

*Mössbauer studies*. $^{57}$Fe Mössbauer spectra were obtained for all samples at 300 and 20 K, using a closed loop refrigerator system. A constant acceleration spectrometer was used to move a $^{57}$Co(Rh) source kept at 300 K. The spectrometer was calibrated with α-Fe and isomer shift values are given relative to this.

The experimental data were fitted by a least-squared computer minimization routine using a sum of spectral components characterizing different iron phases [33].

*Surface area measurements*. The specific surface area of the solids was checked by $N_2$ adsorption (BET) at 77 K using a single point Carlo Erba Sorpty 1750 and a multi-point Fisons Sorpty 1900 system.

### 2.3. Catalytic and transient studies

The catalytic activity tests of solids $La_{1-x-y}Sr_xCe_yFeO_3$ for the NO+CO reaction were carried out in a bench scale tubular plug flow reactor at 1 atm total pressure. The reactor, heating system and the chromatographic analysis of the reactor effluent gas were previously described [12]. The catalysts were tested in the temperature range 280–560°C, at a feed gas composition (mol%) of NO/CO/He=2/2/96, a total flow of 90 scc/min and a constant amount of catalyst, $W$=0.25 g. The GHSV was about 54 000 $h^{-1}$.

The flow system used for conducting catalytic measurements for the $CH_4$/NO/$O_2$ (lean-$NO_x$) reaction at 1 atm total pressure consisted of a flow measuring and control system (MKS Instruments, Model 247C), mixing chambers, a quartz fixed-bed microreactor (2 ml nominal volume) and a GC–MS analysis system. The flow system, the microreactor and the analysis system used have been recently described in detail [34]. The feed stream consisted of 0.5% NO, 0.67% $CH_4$, 5% $O_2$ and He as the balance gas was used in all the experiments. The amount of catalyst sample used was 0.5 g and the total flow rate was 30 scc/min, resulting in a GHSV of about 12 000 $h^{-1}$. Before any measurements were taken, the fresh catalyst sample was pretreated at 700°C in 5%$O_2$/He flow for 2 h.

Nitrogen reaction rates were calculated from the product analyses using the differential reactor approximation, i.e., rate (mol $g^{-1}$ $s^{-1}$)=$N_T y_i/W$, where $N_T$ is the total molar flow rate (mol/s), $y_i$ the molar fraction of component $i$ (i.e., $N_2$) expressed in ppm×$10^{-6}$, and $W$ is the weight of the catalyst (g). For the present catalytic reaction of NO/$CH_4$/$O_2$, methane reacts with NO and $O_2$ according to the following competitive reaction scheme:

$$2NO + CH_4 + O_2 \rightarrow N_2 + CO_2 + 2H_2O \quad (1)$$

$$2NO + O_2 \rightarrow 2NO_2 \quad (2)$$

$$CH_4 + 2O_2 \rightarrow CO_2 + 2H_2O \quad (3)$$

The only N-containing product species formed in the present catalytic reaction system were $N_2$ and $NO_2$. The selectivity, $\alpha$, for $CH_4$ reduction of NO to $N_2$, i.e., the ratio of the consumption rate of $CH_4$ (reaction (1)) to the total one (reaction (1)+reaction (3)) is calculated based on Eq. (4):

$$\alpha\ (\%) = \frac{0.5 y^{f}_{NO} X_{NO}}{y^{f}_{CH_4} X_{CH_4}} \times 100 \quad (4)$$

where $y^{f}_{NO}$ and $y^{f}_{CH_4}$ are the inlet molar fractions of NO and $CH_4$, respectively, while $X_{NO}$ and $X_{CH_4}$ are the NO conversion for reaction (1) and the total $CH_4$ conversion, respectively. The value of 0.5 is the stoichiometric ratio of NO to $CH_4$ (reaction (1)). The fraction of $CH_4$ combusted by $O_2$ (reaction (3)) is given by (100−$\alpha$)/100.

The TOF of the NO reduction by CO or $CH_4$ (lean-$NO_x$ reaction) were calculated after dividing the rate (μmol/g s) by the irreversible NO uptake (μmol/g). The latter amount was determined by TPD experiment (with mass spectrometer as a detector) following adsorption of NO from a 0.5%NO/He mixture at 500°C for 20 min and cooling the reactor to room temperature in NO/He flow before TPD.

TPD experiments were conducted in a specially designed flow-system that has been recently described [34]. Chemical analysis of the gas effluent stream of reactor during transients was done with an *on-line* quadrupole mass spectrometer (Omnistar, Balzers) equipped with a fast response inlet capillary/leak valve (SVI 050, Balzers) and data acquisition systems. The gaseous responses obtained by mass spectrometry were calibrated using standard mixtures. For oxygen and nitric oxide TPD measurements, the mass numbers (*m/z*) 28, 30, 32, 44 and 46 were used for $N_2$, NO, $O_2$, $N_2O$ and $NO_2$, respectively.

## 3. Results

### 3.1. Catalyst characterization

The specific surface area of the ceramic solids was found to be <4 $m^2$/g. Based on this result, specific reaction rates were not calculated per $m^2$ but either

Table 1
Prepared solids, detected crystal phases (XRD) and percentage of Fe-containing crystal phases

| Solid composition | Crystal phases (XRD) | Percentage of Fe-containing crystal phases as determined by Mössbauer at 20 K | | |
|---|---|---|---|---|
| | | $LaFeO_3$ | $Fe_2O_3$ | $SrFeO_{3-x}$ |
| $La_{0.5}Ce_{0.5}FeO_3$ | $LaFeO_3/Fe_2O_3/CeO_2$ | 46 | 54 | |
| $La_{0.5}Sr_{0.2}Ce_{0.3}FeO_3$ | $LaFeO_3/SrFeO_{3-x}/Fe_2O_3/CeO_2/La(OH)_3$[a]$/SrFe_{12}O_{19}$[a] | 37 | 35 | 28 |
| $La_{0.5}Sr_{0.3}Ce_{0.2}FeO_3$ | $LaFeO_3/SrFeO_{3-x}/Fe_2O_3/CeO_2/La(OH)_3$[a]$/SrFe_{12}O_{19}$[a] | 28 | 39 | 33 |
| $La_{0.5}Sr_{0.5}FeO_3$ | $LaFeO_3/SrFeO_{3-x}/SrFeLaO_4$[a]$/La(OH)_3$[a]$/SrFe_{12}O_{19}$[a] | 19 | 36 | 45 |

[a] Traces.

per gram of solid or as TOFs based on the irreversible NO uptake by the solids. The crystal composition of the $La_{1-x-y}Sr_xCe_yFeO_3$ solids as determined by XRD with reference to ASTM standards is shown in Table 1. In the case of $La_{0.5}Ce_{0.5}FeO_3$, the phases apparent were $LaFeO_3$ (perovskite phase) and $CeO_2$ in addition to the major $Fe_2O_3$ phase. In the case of $La_{0.5}Sr_{0.5}FeO_3$, apart from the perovskite-type structure of $SrFeO_{3-x}$ (the main phase), a second perovskite-type phase of $LaFeO_3$ is also apparent. Similar results have also been reported in [35,36]. Traces of additional phases were also found (see Table 1). The double substituted materials with $x+y=0.5$ apart from the two perovskite structures of $LaFeO_3$ and $SrFeO_{3-x}$ contain also the crystal phases of $Fe_2O_3$, $CeO_2$, $SrFe_{12}O_{19}$ and $La(OH)_3$, the latter two phases being in traces (see Table 1).

The Mössbauer spectrum of $La_{0.5}Ce_{0.5}FeO_3$ taken at room temperature revealed the presence of $Fe^{3+}$ with no sign of any other magnetic or paramagnetic component. The spectra of the other solids which contain Sr composed of at least two superimposed six-line patterns and one singlet near zero velocity. The hyperfine parameters, deduced after least squares computer minimization, have shown that the magnetic components correspond to $Fe^{3+}$ and the singlet to $Fe^{5+}$. It was found that the area of the $Fe^{5+}$ component is increasing as the Sr content increases. The Mössbauer spectra taken at 20 K were fully magnetized. From the hyperfine parameters deduced, it was found that all samples contain $LaFeO_3$ and $\alpha$-$Fe_2O_3$ phases. The area corresponding to $LaFeO_3$ was found to increase with increasing Ce content in the sample. On the other hand, the area corresponding to $\alpha$-$Fe_2O_3$ remains practically the same for up to a given Ce content, while it increases at higher Ce contents. These quantitative results are presented in Table 1. From the magnetic components of the spectra observed, the presence of $SrFeO_{3-x}$ phase was also revealed where $Fe^{+3}$ to $Fe^{+5}$ charge disproportionation occurs [37].

### 3.2. Catalyst performance

#### 3.2.1. NO+CO reaction

Fig. 1 shows temperature profiles for the percentage conversion of NO and the selectivity of the NO reduction by CO towards $N_2$ formation over a series of $La_{1-x-y}Sr_xCe_yFeO_3$ solids. At the stated experimental conditions (see Section 2.3), the present materials exhibit significant activity in the tempera-

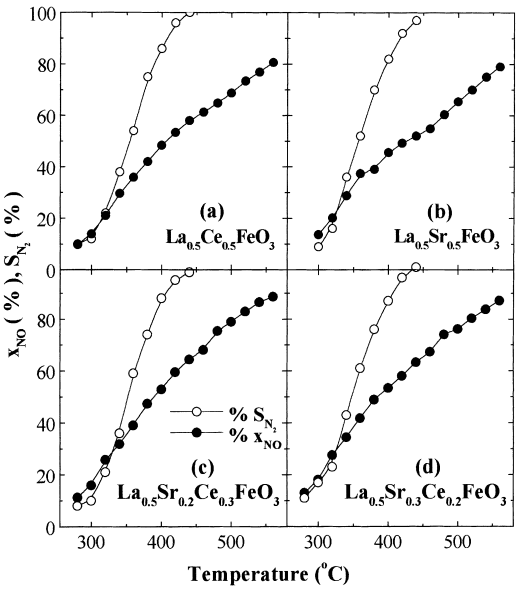


Fig. 1. Temperature profiles for NO conversion (●) and $N_2$ selectivity (○) for the NO+CO reaction on $La_{1-x-y}Sr_xCe_yFeO_3$ solids. NO=2 mol%, CO=2 mol%, $W$=0.25 g, $F$=90 scc/min.

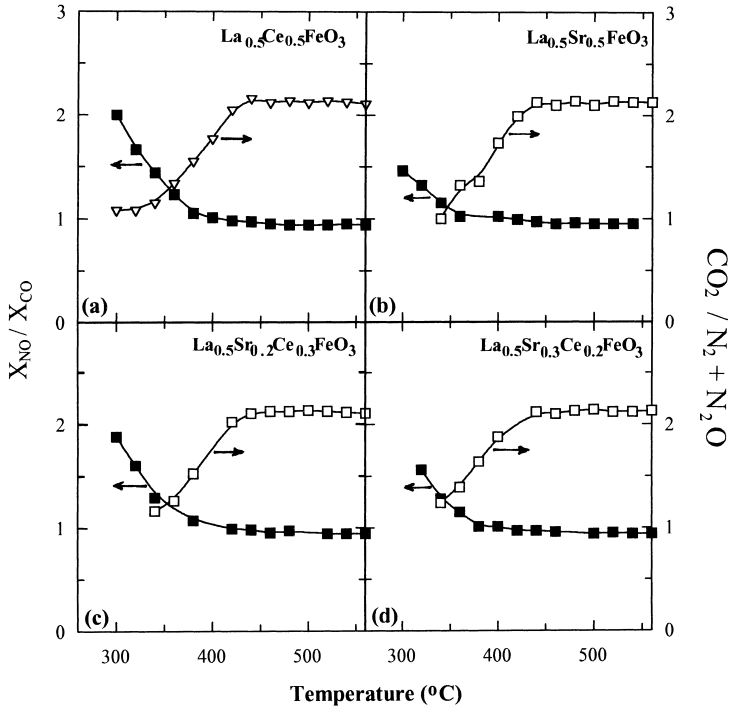


Fig. 2. Ratios of the degrees of conversion $X_{NO}/X_{CO}$ and of the reaction products $CO_2/(N_2+N_2O)$ as a function of reaction temperature on $La_{1-x-y}Sr_xCe_yFeO_3$ solids. NO=2 mol%, CO=2 mol%, $W$=0.25 g, $F$=90 scc/min.

ture range 350–550°C. At temperatures higher than about 425°C, the $N_2$ selectivity is 100%. The only N-containing product species observed are $N_2$ and $N_2O$. Fig. 2 shows temperature profiles of the ratio of NO conversion to that of CO ($X_{NO}/X_{CO}$), as well as of the ratio of $CO_2$ production to that of N-containing species ($N_2+N_2O$). It is clearly seen in Fig. 2 that at low-temperatures the conversion of NO is higher than that of CO, while at temperatures higher than about 400°C, the two reactants tend to react in equal degrees of conversion. This behavior will be discussed later. It is noted that the production of $N_2O$ starts at low temperatures and reaches a maximum at about 320–360°C depending on the composition of the solid. On the other hand, the ratio of $CO_2/(N_2+N_2O)$ takes the value of about unity at low temperatures and increases towards the value of about 2.1 as the temperature of reaction increases. This behavior will also be discussed later.

Fig. 3a presents integral reaction rates of NO consumption (μmol/g s) at $T$=300, 340, 460 and 540°C, while Fig. 3b presents intrinsic reaction rates at $T$=300°C (at $X_{NO}$<20%) in terms of TOF ($s^{-1}$), as a function of catalyst composition. Fig. 3c shows the percentage of the $LaFeO_3$, α-$Fe_2O_3$ and $SrFeO_{3-x}$ crystal phases in all the four materials in order to check any relation of the composition of these solids in the above mentioned phases with their catalytic activity. The doubly substituted perovskite-type materials exhibit higher activities (per gram basis) than the singly substituted ones (Fig. 3a). It is to be pointed out that these differences in activity are not very large. On the other hand, they did not suffered from experimental errors. When the TOF numbers are compared, there is a monotonic decrease in the TOF value with increasing Sr and a corresponding decrease in Ce content of the solid (see Fig. 3b). The decrease is more than double in the TOF value when a comparison is made between the $La_{0.5}Ce_{0.5}FeO_3$ and $La_{0.5}Sr_{0.5}FeO_3$ solids. A nice correlation exists between the TOF values and the percentage of $LaFeO_3$ and $SrFeO_{3-x}$ phases in the solids. The decrease of

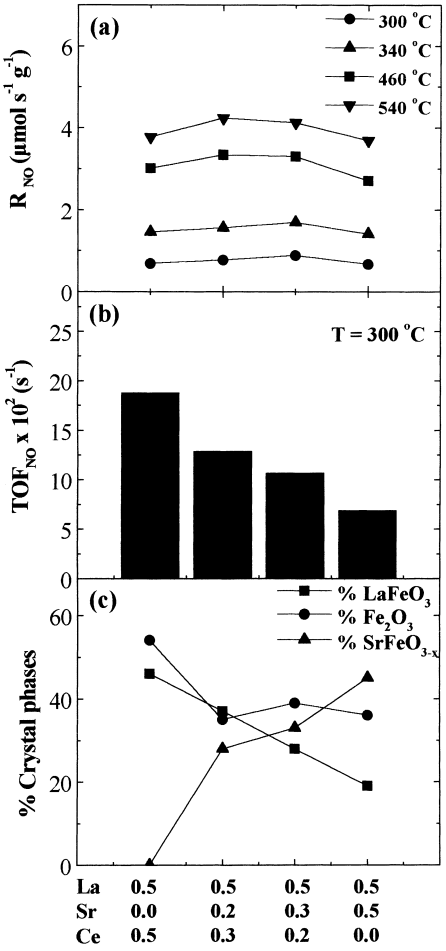


Fig. 3. (a) Integral reaction rates of NO consumption (μmol/g s) as a function of reaction temperature and catalyst composition. (b) TOF ($s^{-1}$) of NO consumption at $T$=300°C as a function of catalyst composition. (c) Composition of $La_{1-x-y}Sr_xCe_yFeO_3$ solids in Fe-containing crystal phases as determined by Mössbauer spectroscopy at 20 K.

the TOF value with increasing Sr content in the solid correlates with the simultaneous increase of $SrFeO_{3-x}$ and the decrease of $LaFeO_3$ phase in the solid.

Fig. 4 presents values of the apparent activation energies of $N_2$ and $N_2O$ formation as a function of solid composition. These apparent activation energy values were calculated based on the graph of ln $R$ vs. $1/T$, where $R$ is the intrinsic reaction rate (μmol/g s) of $N_2$ or $N_2O$ formation in the temperature range 280–340°C. Values in the range 110–165 kJ/mol for the $N_2$ formation and 40–60 kJ/mol for the $N_2O$ formation were calculated. These results are in harmony with the observations that in this low-temperature range of reaction, the $N_2$ selectivity is relatively low.

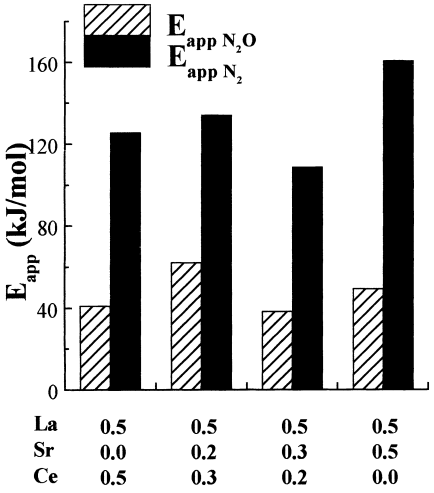


Fig. 4. Apparent activation energies (kJ/mol) for the formation of $N_2$ and $N_2O$ during the NO+CO reaction as a function of catalyst composition. NO=2 mol%, CO=2 mol%, $W$=0.25 g, $F$=90 scc/min, $T$=280–340°C.

### 3.2.2. $NO+CH_4+O_2$ (lean-$NO_x$) reaction

The catalytic behavior of $La_{1-x-y}Sr_xCe_yFeO_3$ solids for the reduction of NO in the presence of excess of oxygen using $CH_4$ as a reducing agent is presented in Fig. 5A. Catalytic results are given in terms of rate of $N_2$ production (μmol/g s) in the temperature range 250–550°C. All catalysts exhibit a maximum in the rate of reaction in the range 370–400°C, depending on catalyst composition, except the $La_{0.5}Ce_{0.5}FeO_3$ catalyst that shows a local maximum at about 450°C (Fig. 5A). The highest reaction rate was obtained with $La_{0.5}Sr_{0.2}Ce_{0.3}FeO_3$ catalyst (Fig. 5A, curve b) at 400°C. This catalyst also exhibits the highest reaction rates in the range 370–550°C, but lower rates at $T$<370°C as compared to the other three catalysts in the series. It is noted that the highest reaction rate observed over $La_{0.5}Sr_{0.2}Ce_{0.3}FeO_3$ catalyst corresponds to 25.5% NO conversion and 93.1% $N_2$ selectivity. The selectivity behavior of all four samples was found to be similar. Values for the $N_2$ selectivity at $T$=250, 350, 450 and 550°C are 78, 88, 95 and 100%, respectively, for the $La_{0.5}Sr_{0.2}Ce_{0.3}FeO_3$ catalyst.

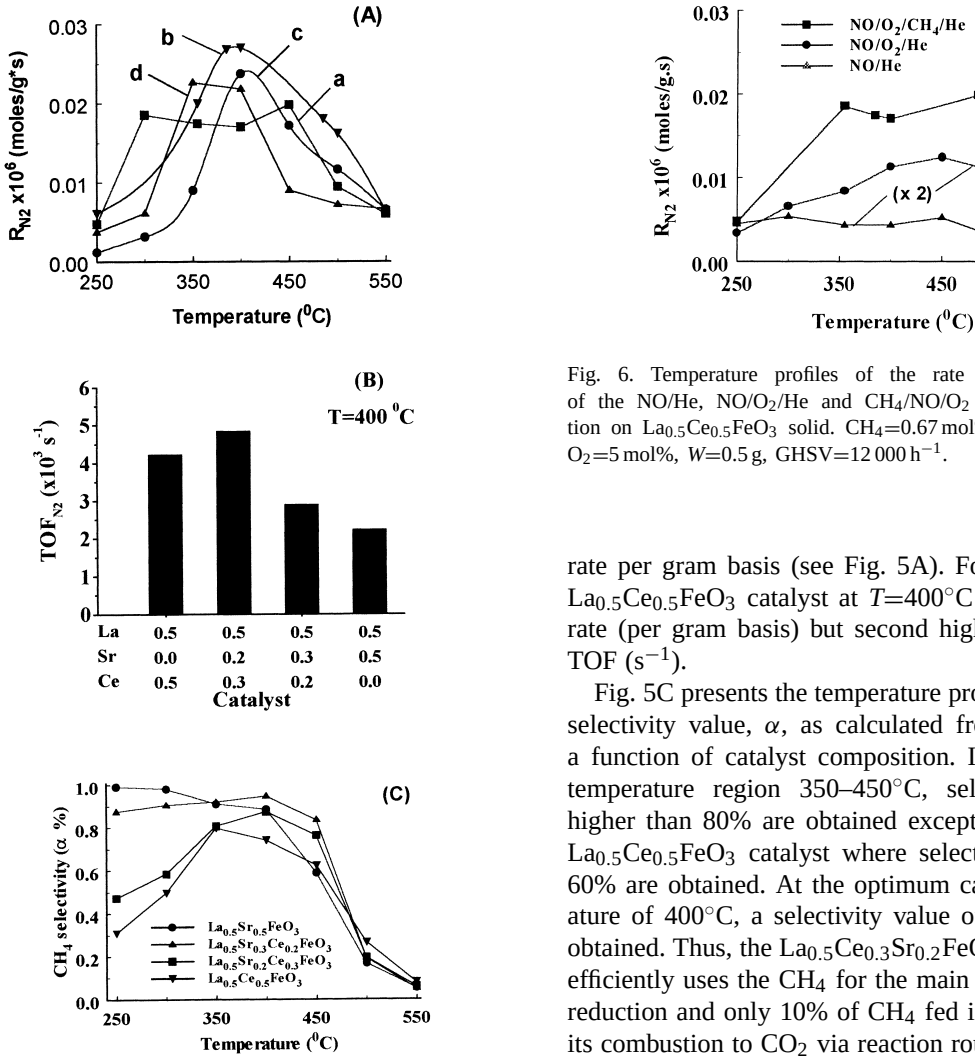


Fig. 5. (A) Temperature profiles of the rate of $N_2$ formation of the $CH_4/NO/O_2$ "lean-$NO_x$" reaction as a function of catalyst composition. (B) TOF ($s^{-1}$) of $N_2$ formation at 400°C as a function of catalyst composition. (C) Temperature profile of the $CH_4$ selectivity value, $\alpha$ (%), of the $CH_4/NO/O_2$ "lean-$NO_x$" reaction as a function of catalyst composition. $CH_4$=0.67 mol%, NO=0.5 mol%, $O_2$=5 mol%, $W$=0.5 g, GHSV=12 000 $h^{-1}$.

Fig. 5B compares the activity of the present four catalysts in terms of TOF ($s^{-1}$) for $N_2$ production at $T$=400°C. The $La_{0.5}Sr_{0.2}Ce_{0.3}FeO_3$ catalyst remains the most active, having the highest intrinsic site reactivity, while the order of activity for the other three catalysts is now different from that based on the




Fig. 6. Temperature profiles of the rate of $N_2$ formation of the NO/He, $NO/O_2$/He and $CH_4/NO/O_2$ "lean-$NO_x$" reaction on $La_{0.5}Ce_{0.5}FeO_3$ solid. $CH_4$=0.67 mol%, NO=0.5 mol%, $O_2$=5 mol%, $W$=0.5 g, GHSV=12 000 $h^{-1}$.

rate per gram basis (see Fig. 5A). For example, the $La_{0.5}Ce_{0.5}FeO_3$ catalyst at $T$=400°C has the lowest rate (per gram basis) but second higher in terms of TOF ($s^{-1}$).

Fig. 5C presents the temperature profile of the $CH_4$ selectivity value, $\alpha$, as calculated from Eq. (4), as a function of catalyst composition. In the optimum temperature region 350–450°C, selectivity values higher than 80% are obtained except in the case of $La_{0.5}Ce_{0.5}FeO_3$ catalyst where selectivity values of 60% are obtained. At the optimum catalytic temperature of 400°C, a selectivity value of about 90% is obtained. Thus, the $La_{0.5}Ce_{0.3}Sr_{0.2}FeO_3$ catalyst very efficiently uses the $CH_4$ for the main reaction of NO reduction and only 10% of $CH_4$ fed is consumed for its combustion to $CO_2$ via reaction route (3).

In order to demonstrate the ability of $CH_4$ to largely enhance the reduction of NO, catalytic experiments were also performed with feed mixtures of 0.5%NO/He and 0.5%NO/5%$O_2$/He over the $La_{0.5}Ce_{0.5}FeO_3$ catalyst. Fig. 6 presents the results obtained in terms of reaction rate towards $N_2$ formation as a function of reaction temperature. The first comment to be made is that the presence of 5% $O_2$ in the feed significantly promotes the NO decomposition reaction. On the other hand, addition of $CH_4$ in the $NO/O_2$/He feed further enhances the rate of reaction. At 350°C, an enhancement factor of about 8 is obtained when the rate of $N_2$ formation is compared between the NO/He and $NO/O_2/CH_4$/He feed mixtures.

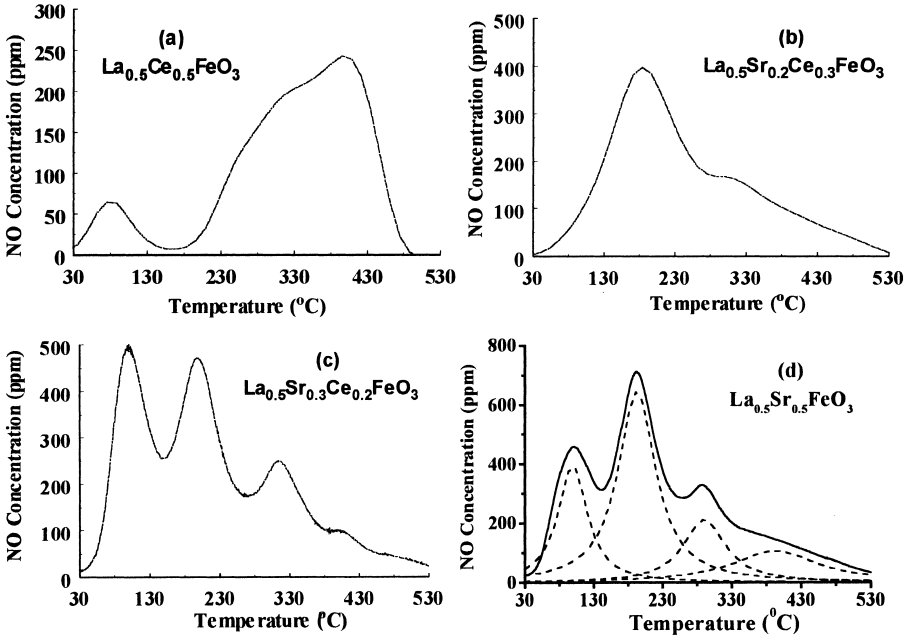


Fig. 7. TPD profiles of NO on $La_{1-x-y}Sr_xCe_yFeO_3$ solids ($x$=0.2, 0.3; $y$=0.3, 0.2, respectively).

### 3.3. TPD studies

Fig. 7 presents TPD profiles of NO as a function of catalyst composition. The interaction of NO over these solids varies significantly as clearly shown in Fig. 7a–d. In the case of $La_{0.5}Ce_{0.5}FeO_3$, two distinct desorption peaks appear. The first small peak is centered at 75°C, while the second large peak at 410°C with a shoulder at the rising part of it. As Ce is substituted by Sr, desorption of NO at $T$<250°C increases significantly, while the opposite occurs for the high-temperature desorption peak (compare Fig. 7a and b). Further substitution of Ce by Sr results in a totally different desorption behavior of NO. Three distinct desorption peaks are now observed with a shoulder at the falling part of the high-temperature desorption peak (Fig. 7c). In addition, desorption of NO in the low temperature range 30–250°C significantly increases with respect to the $La_{0.5}Ce_{0.5}FeO_3$ sample. The amounts of NO desorbed as a function of catalyst composition are reported in Table 2. Complete substitution of Ce by Sr ($La_{0.5}Sr_{0.5}FeO_3$) results in small changes in the TPD profile of NO with respect to the $La_{0.5}Sr_{0.3}Ce_{0.2}FeO_3$ case (compare Fig. 7c and d). An important result is the fact that there is a monotonic increase in the amount of NO chemisorption with increasing substitution of Ce by Sr in the $La_{1-x-y}Sr_xCe_yFeO_3$ solids as Table 2 indicates. Deconvolution of the TPD profile of NO obtained over the $La_{0.5}Sr_{0.5}FeO_3$ solid is presented in Fig. 7d. The

Table 2
Amounts of $O_2$ and NO desorbed from $La_{0.5}Sr_xCe_yFeO_3$ after TPD experiments of $O_2$ and NO

| Catalyst | Amount of $O_2$ desorbed[a] ($\mu$mol g$^{-1}$) | Amount of NO desorbed ($\mu$mol g$^{-1}$) |
|---|---|---|
| $La_{0.5}Ce_{0.5}FeO_3$ | 3.2 (0.2) | 3.6 |
| $La_{0.5}Sr_{0.2}Ce_{0.3}FeO_3$ | 93.0 (5.4) | 6.0 |
| $La_{0.5}Sr_{0.3}Ce_{0.2}FeO_3$ | 182.4 (11.2) | 8.2 |
| $La_{0.5}Sr_{0.5}FeO_3$ | 236.8 (14.5) | 9.8 |

[a] Number in parentheses corresponds to equivalent surface oxygen monolayers (based on BET=4 m$^2$/g).

use of Lorentzian peak shapes in a computer peak fitting routine (first order desorption kinetics for NO) resulted in a nice curve fitting of the experimental results with four desorption peaks (Fig. 7d).

Fig. 8 presents TPD profiles of $O_2$ as a function of catalyst composition. As in the case of NO desorption (Fig. 7), drastic changes occur on the adsorption and desorption characteristics of $O_2$ when Ce is progressively substituted by Sr. A single small desorption peak of $O_2$ is observed on $La_{0.5}Ce_{0.5}FeO_3$ sample (Fig. 8a), while five desorption peaks are observed on $La_{0.5}Sr_{0.5}FeO_3$ (Fig. 8d) with a total $O_2$ chemisorption amount 75 times higher than that observed on the $La_{0.5}Ce_{0.5}FeO_3$ solid. The amount ($\mu$mol/g) of $O_2$ desorbed as a function of catalyst composition is given in Table 2. In parentheses the number of equivalent surface oxygen monolayers (based on a BET=4 $m^2$/g) is also indicated. Numbers greater than unity are apparent, a result indicating that desorption of subsurface lattice oxygen species takes place via bulk diffusion from the crystal to its surface. From Table 2 it is clearly seen that there is a monotonic increase in the uptake of $O_2$ as the Ce content in the $La_{0.5}Ce_{0.5}FeO_3$ sample is substituted by Sr. This behavior will also be discussed next.

A remarkable result observed during the $O_2$ TPDs over the present solids is that the presence of Sr induces an oscillatory behavior in the rate of desorption of $O_2$. This oscillatory behavior is clearly demonstrated in Fig. 8b for the case of $La_{0.5}Sr_{0.2}Ce_{0.3}FeO_3$ solid, where it appears to be more intense at temperatures higher than 550°C. An oscillatory behavior has also been observed at $T$>650°C on the $La_{0.5}Sr_{0.5}FeO_3$ solid (not clearly seen in Fig. 8d due to the scale unit). The oscillatory behavior observed during $O_2$ TPD in the present solids will be discussed next.

## 4. Discussion

### 4.1. NO+CO reaction

#### 4.1.1. The $X_{NO}/X_{CO}$ and $CO_2/(N_2+N_2O)$ behavior

In line with previous studies [8,9,11–13], the reaction between NO and CO proceeds via either one of the following two routes:

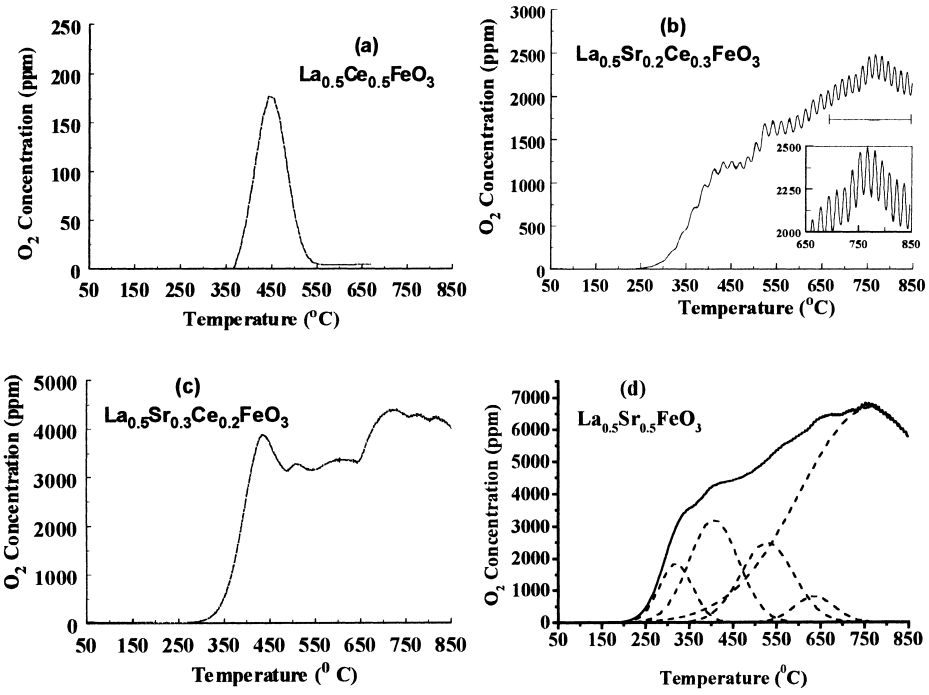


Fig. 8. TPD profiles of $O_2$ on $La_{1-x-y}Sr_xCe_yFeO_3$ solids ($x$=0.2, 0.3; $y$=0.3, 0.2, respectively).

$$\text{Route 1}: \quad 2NO + 2CO \rightarrow N_2 + 2CO_2 \tag{5}$$

$$\text{Route 2}: \quad 2NO + CO \rightarrow N_2O + CO_2 \tag{6}$$

For route 1, the ratio of conversion of NO and CO must be equal to 1, while the molecular ratio of $CO_2$ and $N_2$ reaction products must be equal to 2. For route 2, the ratio of the degrees of conversion $X_{NO}/X_{CO}$ must be equal to 2, while the molar ratio $CO_2/(N_2+N_2O)$ must be equal to 1. Based on this analysis and the experimental results of Fig. 2, it is safe to conclude that at reaction temperatures higher than 400°C, route 1 is exclusively dominant over route 2. On the other hand, the experimental ratio $CO_2/(N_2+N_2O)$ ought to take the value of 2 according to what is mentioned above. The relatively small deviation (about 5–8%) of the observed experimental value from the theoretical one could at first be explained based on additional reaction routes. A possible alternative route might be the following one:

$$\text{Route 3}: \quad N_2O + CO \rightarrow N_2 + CO_2 \tag{7}$$

However, combination of all three reaction routes gives an upper limit value 2 for the $CO_2/(N_2+N_2O)$ ratio. It is therefore concluded that the reported values of the latter parameter being greater than 2 suffer from experimental errors in quantifying the $N_2$, $N_2O$ and $CO_2$ reaction products. On the other hand, it must be pointed out that the use of $CO_2/(N_2+N_2O)$ ratio in order to explain the catalytic results of the NO+CO reaction is much more useful than the use of $CO_2/N_2O$ ratio. This is because the latter ratio cannot discriminate between reaction routes 1 and 3. For example, if reaction route 2 is only responsible for the production of $N_2O$, then the ratio of $CO_2/N_2O$ is always greater than unity independent of the presence of reaction route 1 or 3 or both of them.

#### *4.1.2. The influence of crystal phases in promoting catalytic activity*

Table 1 and Fig. 3c present quantitative results of the three main Fe-containing crystal phases found in $La_{1-x-y}Sr_xCe_yFeO_3$ solids as well as the identity of other crystal phases present (e.g., $CeO_2$). The measured activity reflects only that of crystal phases present that are able to catalyze the NO+CO reaction. It is therefore important in the mixed oxidic/perovskitic catalytic systems to stress the intrinsic site reactivity and relate this to the composition of the crystal phases present. This was done by evaluating the site reactivity (TOF) of the materials and plotting it against catalyst composition (Fig. 3b). It is noted that this way of evaluation assumes that the NO chemisorption site is the most important site of the catalytic cycle. It was found that $La_{0.5}Ce_{0.5}FeO_3$ catalyst has the highest TOF at 300°C as compared to the other three materials tested. This catalyst was found to contain the highest percentage in $LaFeO_3$ and $\alpha$-$Fe_2O_3$ phases (see Fig. 3c). In addition, it was found to possess the largest ratio in the XRD intensities of the main peaks of $CeO_2$ and $LaFeO_3$ phases. On the other hand, Fig. 3a shows a different activity order in terms of integral reaction rate or conversion of NO as compared to the TOF activity order (Fig. 3b). It is suggested that the addition of Sr for Ce results in an increasing number of exposed active sites per gram of solid due to an increased BET area of the crystal phases formed with respect to that of the phases found in $La_{0.5}Ce_{0.5}FeO_3$ solid. However, the site reactivity of $SrFeO_{3-x}$ phase seems to be lower than that exhibited by the crystal phases present in the $La_{0.5}Ce_{0.5}FeO_3$ solid. Thus, the increase of the BET area of the active phases present in the $La_{0.5}Ce_{0.5}FeO_3$ system is expected to result in higher NO conversions as compared to the other materials in the series.

Catalytic measurements performed over the parent perovskite material of $LaFeO_3$ and $Fe_2O_3$ for the same reaction conditions [12,38] indicate that the Ce- and Sr-containing materials ($La_{1-x-y}Sr_xCe_yFeO_3$) appear twice as active (at low temperatures) as the $LaFeO_3$ and $Fe_2O_3$ pure phases. Martìnez-Arian et al. [39] have suggested that the remarkable activity of $CuO_x/CeO_2$ catalysts for CO oxidation, as compared to the activity of conventional $Cu/Al_2O_3$ catalyst, could be explained by invoking a synergistic effect between the Cu and Ce binary oxides. The $Cu^+$ species provide the sites for CO adsorption, while $CeO_2$ acts as an oxygen-supply source. Based on these results, a synergy phenomenon between the $CeO_2$ and the other two phases present in the $La_{0.5}Ce_{0.5}FeO_3$ catalytic system may contribute to the high TOF number exhibited by this material. For instance, a spill-over of adsorbed NO on one phase onto more active sites for reduction in another phase. Based on the $O_2$ chemisorption results obtained by TPD (see Table 2), $La_{0.5}Ce_{0.5}FeO_3$ has the lowest concentration of

oxygen vacancies. In particular, the oxygen chemisorption on $La_{0.5}Ce_{0.5}FeO_3$ is found to be 60 times lower than that measured on $La_{0.5}Sr_{0.2}Ce_{0.3}FeO_3$. In addition, the decreasing activity order in terms of TOF (Fig. 3b) coincides with the increasing $O_2$ chemisorption uptake measurements. These results may point out the importance of oxygen vacancies in controlling the activity of NO/CO reaction. Dependence of the catalytic activity of various reactions on the concentration of oxygen vacancies over $SrMO_{3-x}$ has also been proposed by other investigators [35,36,40].

#### *4.1.3. Comparison of the activity of the present and other perovskite-type materials*

A large number of studies have appeared in the literature concerning the reduction of NO by CO over a variety of catalyst compositions. In general, it can be said that perovskite-type materials exhibit satisfying activity, stability with time on stream and poisoning resistance to $SO_2$, especially in the low-temperature range 200–450°C. On the other hand, noble metals are considered superior to perovskites for the present reaction system when the conversion of NO at the same reaction conditions is concerned.

Table 3 attempts to present the literature data concerning various perovskite-type materials that exhibit significant catalytic activity for the NO/CO reaction in the low-temperature range 200–450°C. Also in Table 3 are cited data for the $Rh/Al_2O_3$ catalyst for comparison purposes, and when possible, the intrinsic site reactivity of the catalysts is reported. Based on the results of Table 3, the present $La_{0.5}Sr_{0.3}Ce_{0.2}FeO_3$ and $La_{0.5}Sr_{0.2}Ce_{0.3}FeO_3$ catalysts exhibit one of the highest activities in terms of integral rates of NO conversion per gram of solid basis. More importantly, they exhibit the highest site reactivity (TOF) among all perovskites listed in Table 3, and a comparable TOF value (site reactivity) with the $Rh/Al_2O_3$ catalyst. The latter is an important result of this comparison since it gives the incentive for the preparation of perovskites of similar composition but of higher specific surface areas, thus leading to higher integral reaction rates.

Table 3
Catalytic activity of various mixed oxidic/perovskitic materials for the NO+CO reaction in the low-temperature range 200–450°C

| Serial No. | Catalyst | Experimental conditions | $T$ (°C) | $R_{NO}\times10^6$ (mol/s $g_{cat}$) | $TOF_{NO}$ ($s^{-1}$)$\times10^3$ $X_{NO}<20\%$ | Ref. |
|---|---|---|---|---|---|---|
| 1 | $La_{0.5}Sr_{0.5}CoO_3$ | NO=5000 ppm; CO=4000 ppm SV=50 000 $cm^3\,h^{-1}\,g^{-1}$ | 340 | 1.42 | | [17] |
| 2 | $LaFeO_3$ | NO=1500 ppm; CO=1500 ppm | 260 | 0.20 | 0.158[b] (230°C) | [35] |
| | $La_{0.5}Sr_{0.5}FeO_3$ | $W$=0.3 g; $F$=120 $cm^3$/min | 340 | 0.20 | 0.254[b] (300°C) | |
| 3 | $LaMnO_3$ | 2% NO; 2% CO | 350 | 0.69 | | [41] |
| | $LaMn_{0.99}Pt_{0.01}O_3$ | $W/F$=4 g h $mol^{-1}$; $W$=1 g | 260 | 0.69 | | |
| 4 | $Bi_2Sr_2CaCu_2O_y$ | 8% NO; 8% CO, $W$=50 mg | 300 | 1.50 | | [42] |
| | $YBa_2Cu_3O_y$ | | 300 | 1.20 | | |
| 5 | $LaMn_{0.6}Cu_{0.4}O_3$ | 8% NO; 8% CO, $W$=50 mg | 300 | 2.8 | | [43] |
| 6 | $La_2CuO_4/ZrO_2$ | 8% NO; 8% CO, $W$=50 mg | 200 | 1.67 | 18[a] | [44] |
| 7 | $La_{0.8}Sr_{0.2}CoO_3$ | 0.5% NO; 0.5% CO | 400 | 0.26 | | [11] |
| | $La_{0.8}Sr_{0.2}Co_{0.9}Cu_{0.05}Ru_{0.05}O_3$ | $W$=0.2 g; $F$=30 $cm^3$/min | 440 | 0.26 | | |
| 8 | $LaCoO_3$ | 8% NO; 8% CO, $W$=50 mg | 300 | 1.24 | | [9] |
| | $LaFeO_3$ | | 300 | 2.00 | | |
| | $LaMnO_3$ | | 300 | 0.70 | | |
| | $La_{0.9}Sr_{0.1}FeO_3$ | | 300 | 0.85 | | |
| | $La_{0.8}Sr_{0.2}CoO_3$ | | 300 | 0.61 | | |
| 9 | $La_{0.5}Sr_{0.3}Ce_{0.2}FeO_3$ | 2% NO; 2% CO; $F$=90 $cm^3$/min | 300 | 0.90 | 107[b] | This work |
| | $La_{0.5}Sr_{0.2}Ce_{0.3}FeO_3$ | $W$=0.25 g | 300 | 0.80 | 129[b] | |
| 10 | $Rh/\alpha\text{-}Al_2O_3$ (3 wt.%) | 0.5% NO; 1% CO $F$=5000 $cm^3$/min; $W$=3 g | 230 | 2.2 | 79.0[c] | [22] |

[a] Mole of NO converted/(total Cu-atom×s).
[b] Mole of NO converted/(mole NO adsorbed×s).
[c] Mole of NO converted/(mole of exposed Rh×s).

An interesting result of Table 3 is that while Sr substitution for La in the $LaFeO_3$ [35] resulted in a catalyst of lower activity (a higher $T$ is required to obtain the same reaction rate), the opposite result is seen in the present case of $La_{0.5}Ce_{0.5}FeO_3$ mixed oxidic/perovskitic system.

### 4.2. $NO+CH_4+O_2$ reaction

There is very little work performed for the reduction of NO in the presence of excess oxygen ("lean-$NO_x$") using hydrocarbons as reducing agents over perovskite-type materials [1,2]. Agarwal et al. [17] have reported that $La_{0.5}Sr_{0.5}CoO_3$ perovskite was active for the 0.4%$CH_4$/0.42%NO/He reaction only at $T$>600°C. Addition of $O_2$ in the feed mixture had a strong inhibiting effect. More work on "lean-$NO_x$" reduction by hydrocarbons over perovskites has been conducted using $C_3H_6$. Furukawa et al. [25] have reported activities of several perovskite-type solids for the $C_3H_6$/NO/$O_2$ reaction. Significant conversions of NO to $N_2$ ($X_{NO}$=14–21%) were obtained only at high temperatures ($T$=600°C) over $LaAlO_3$, $La_{0.8}Sr_{0.2}AlO_3$ and $LaAl_{0.9}Mg_{0.1}AlO_3$ solids. Recently, Menezo et al. [16] have performed catalytic activity tests for the $C_3H_6$/NO/$O_2$/$H_2O$ reaction over $La_{0.59}Sr_{0.39}MnO_3$ in the temperature range 250–500°C. A maximum NO conversion to $N_2$ of 5% at 350°C has been reported.

According to the above literature survey of "lean-$NO_x$" over perovskite-type materials and the present catalytic activity measurements (Fig. 5), the $La_{1-x-y}Sr_xCe_yFeO_3$ solids compete very favorably among the other perovskite materials reported. In particular, for the $CH_4$/NO/$O_2$ reaction the present mixed oxidic/perovskitic materials investigated are the only ones reported with significant activity in the low-temperature range 250–450°C. Table 4 is an attempt to present and compare the $CH_4$/NO/$O_2$ low-temperature "lean-$NO_x$" activity of various

Table 4
$CH_4$/NO/$O_2$ "lean-$NO_x$" catalytic reaction in the low temperature range 250–450°C

| Serial No. | Catalyst | Experimental conditions | $T$ (°C) | Rate$N_2$ (mol $g_{cat}^{-1}$ $s^{-1}$)×$10^8$ | $TOF_{N_2}$ ($s^{-1}$)×$10^3$ | Reference |
|---|---|---|---|---|---|---|
| 1 | Co-ZSM5 | $CH_4$=1000 ppm; NO=1640 ppm $O_2$=4%, $W$=0.4 g, $F$=100 $cm^3$/min | 360 | 2.2 | – | [45] |
| 2 | Co-ZSM5 | $CH_4$=1015 ppm; NO=1610 ppm $O_2$=2.5%, GHSV=30 000 $h^{-1}$ | 450 | 36.1 | 0.26[a] | [46] |
| 3 | Co-ferrierite | $CH_4$=1015 ppm; NO=1610 ppm $O_2$=2.5%, GHSV=30 000 $h^{-1}$ | 450 | 51.3 | 0.34[a] | [46] |
| 4 | Ga-H-ZSM5 | $CH_4$=1000 ppm; NO=1610 ppm $O_2$=2.5%, GHSV=30 000 $h^{-1}$ $W$=0.1 g, $F$=100 $cm^3$/min | 350<br>400 | 3.6<br>10.2 | –<br>– | [47] |
| 5 | Mn-ZSM5 | $CH_4$=0.5%; NO=0.5% $O_2$=2.0%, $F$=100 $cm^3$/min GHSV=15 000 $h^{-1}$, $W$=0.2 g | 400 | 8.3 | – | [48] |
| 6 | $La_2O_3$ | $CH_4$=0.4%; NO=0.4% $O_2$=4%, $F$=100 $cm^3$/min, $W$=0.1 g | 450 | 2.7 | – | [49] |
| 7 | $La_{0.5}Sr_{0.2}Ce_{0.3}FeO_3$ | $CH_4$=0.67%; NO=0.5%, $O_2$=5% $F$=30 $cm^3$/min, $W$=0.5 g | 300<br>400 | 2<br>2.7 | 3.3[b]<br>4.54[b] | This work |
| 8 | $La_{0.59}Sr_{0.39}MnO_3$ | $C_3H_6$=530 ppm; NO=1200 ppm $O_2$=5%, $H_2O$=10% $F$=166 $cm^3$/min, $W$=0.5 g | 350 | 0.74 | | [16] |
| 9 | $Pt/SiO_2$ (1 wt.%) | $C_3H_6$=1000 ppm; NO=500 ppm $O_2$=5%, $F$=200 $cm^3$/min, $W$=0.1 g | 220<br>300<br>400 | 24.3 ($X_{NO}$=63%)<br>11.2 ($X_{NO}$=30%)<br>3.0 ($X_{NO}$=8%) | <br><br>1.7[c] | [50] |

[a] Moles of $N_2$ produced per moles $Co^{+2}$ exchanged per second.
[b] Based on NO chemisorption (mol/$g_{cat}$).
[c] Based on exposed surface Pt atoms.

materials with significant catalytic activity. Whenever possible, the intrinsic site reactivity (TOF, $s^{-1}$) of the catalyst is also reported. At 300°C, the TOF of the present $La_{0.5}Sr_{0.2}Ce_{0.3}FeO_3$ system is about 13 times higher than that reported over Co-ZSM5 at 450°C. In spite of the higher partial pressures of $CH_4$ and NO used in the present work than in Co-ZSM5 [46], it is clear that the site reactivity of the present materials is at least comparable to that obtained over Co-ZSM5, one of the most active catalysts reported for this reaction. According to the results of Table 4, the present La-containing solids are considered equally active as the pure $La_2O_3$. However, it is important to point out that the $La_2O_3$ catalyst has shown no activity at $T<450$°C, a result opposite for the present materials that show significant activity at $T<450$°C.

An interesting and important result of Table 4 is that related to the TOF value of $Pt/SiO_2$ catalyst for the $C_3H_6/NO/O_2$ reaction at 400°C. The TOF value reported is about 2.5 times lower than the value reported for the present materials. Even though this comparison is made based on different hydrocarbon species and feed conditions, it can be said that if the number of active sites per gram of solid increases significantly, then the present catalyst formulations could be considered as serious competitors of Pt, a relatively rare and expensive metal. This can be achieved by preparing solid materials of the present composition with higher specific surface areas. It is also appropriate to point out that the ability of $C_3H_6$ to reduce NO under "lean-$NO_x$" conditions was found to be higher than $CH_4$ mainly due to the higher C–H bond strength of the latter [50]. This information gives to the present materials even higher credibility for their suitability for low-temperature "lean-$NO_x$" applications.

### *4.3. NO TPD studies*

Infrared spectroscopic studies of NO adsorption have been carried out over $LaFeO_3$ perovskite material [51]. Various infrared bands observed were assigned to (a) dinitrosyl species chemisorbed on $Fe^{2+}$ or $Fe^{3+}$, (b) mononitrosyls adsorbed on $Fe^{2+}$ and $Fe^0$, (c) monodentate, bridged and bidentate nitrates all interacting with iron ions, and (d) nitrite adsorbed structures associated with $La^{3+}$ ions. It was found that the concentration of the various nitrate species increased with increasing adsorption temperature. Similar results were observed upon adsorption of NO on $LaMnO_3$ [52]. The simultaneous presence of nitrosyl and nitrate bands evidences the interaction of NO with cations and oxygen anions as well. Voorhoeve et al. [14] have studied the molecular and dissociative adsorption of NO on $La_{0.8}K_{0.2}MnO_3$. Following $NO/CO/H_2$ reaction, NO was adsorbed at 150°C followed by TPD. Desorption of molecular NO resulted in a peak in the range 150–200°C indicating the presence of moderately strongly chemisorbed NO as a nitrosyl group, presumably on low-valency metal ions [14].

In the present work, TPD of NO on $La_{1-x-y}Sr_xCe_yFeO_3$ solids, following adsorption at 400°C and cooling of the sample in NO/He to room temperature, resulted in several desorption peaks depending on the catalyst composition (Fig. 7a–d). In the case of $La_{0.5}Sr_{0.5}FeO_3$, four peaks ($T_M$=100, 200, 290 and 390°C) have nicely been fitted to the observed experimental TPD spectrum that exhibited three distinct peak maxima and a high-temperature shoulder. An attempt is made to correlate these four peaks with the phase composition of the solids. The first peak appears only in a small amount in the first two samples (Fig. 7a and b), while it drastically increases on the other two samples that contain higher amounts of Sr (Fig. 7c and d). It is suggested that this first NO TPD peak ($T_M$=100°C) is largely due to specific adsorption sites on $SrFeO_{3-x}$ phase which are populated at higher Sr contents (e.g., $y\geq0.3$) in the solid. Such adsorption sites could be oxygen coordinated to cationic defects, $Fe^{5+}$ or oxygen vacancies, the concentration of which becomes significant at Sr contents greater than a given value. The evolution in the amount of the second peak ($T_M$=200°C) correlates very well with the increasing content of Sr in the catalyst. This in turn correlates with the increasing amount of $SrFeO_{3-x}$ phase in the solid (see Table 1). Based on the TPD results of Voorhoeve et al. [14], it is speculated that this NO adsorbed species may correspond to nitrosyl group on $Sr^{2+}$ cations. The third desorption peak ($T_M$=290°C) seems to correlate with the $Fe_2O_3$ crystal phase since its peak maximum intensity changes only slightly upon substitution of Ce by Sr (compare Fig. 7b–d). The fourth NO desorption peak with the highest peak maximum temperature ($T_M$=390°C) seems also to correlate very well with adsorption of NO on the $Fe_2O_3$ phase. Its peak

maximum intensity largely decreases after substitution of Ce by Sr (0.2) and then remains practically constant. This result is in harmony with the behavior in the amount of $Fe_2O_3$ in the series of solids investigated (see Table 1). It should be noted that a small chemisorbed amount of NO on $CeO_2$, the latter being present in the solid composition (Fig. 7a–c), cannot be excluded. However, the main NO chemisorption occurs on the phases previously discussed according to the TPD profiles (Fig. 7a–d) and the phase composition of solids detected (see Table 1).

### 4.4. $O_2$ TPD studies

The effects of partial substitution of $La^{3+}$ by $Sr^{2+}$ in $La_{1-x}Sr_xMO_{3+\delta}$ (M=Co, Fe, Mn) solids on the oxygen chemisorption behavior have been studied by means of the TPD technique [53–55]. In these studies, oxygen was preadsorbed by cooling the sample from 800°C to room temperature in an oxygen atmosphere (100 Torr of $O_2$). In the case of Co-containing perovskite materials, the TPD responses were characterized by the appearance of two desorption peaks, namely α and β adsorption states. The α-state resulted in a broad plateau-like peak appearing in the range 150–750°C, while the β-state resulted in a very sharp peak centered around 820°C. For the unsubstituted sample, only a small β-state desorption peak appeared, while by increasing the $Sr^{2+}$ addition both desorption states were increased. In addition, the total amount of $O_2$ desorbed was found to increase with increasing $Sr^{2+}$ content [53]. The above-mentioned TPD results were explained as follows. The substitution of trivalent La by divalent Sr requires charge compensation. This can be achieved either by the formation of tetravalent Co or positive holes. This in turn results in the formation of oxygen species having broadly dispersed states ($O^{n-}$ species); the latter was confirmed by XPS studies [53]. Seiyama et al. [53] have suggested that the β adsorbed state is more specific to the B-cationic site, though it is also affected by A site substitution [54]. The α adsorption state was suggested to be associated with the oxygen vacancies, the concentration of which increases with increasing Sr addition, while the β adsorption state results in the reduction of B-cationic sites to lower valencies upon oxygen desorption.

Zhang et al. [56] have investigated the oxygen adsorption and desorption properties of doubly substituted (in A and B positions) perovskite-type $La_{1-x}Sr_xCo_{1-y}Fe_yO_3$ solids. A TPD response very similar to the one observed in this work on $La_{0.5}Sr_{0.3}Ce_{0.2}FeO_3$ (Fig. 8c) was also observed in the case of $La_{0.6}Sr_{0.4}Co_{0.4}Fe_{0.6}O_3$ [56]. However, in the absence of Sr, a small oxygen TPD peak was observed at temperatures higher than 700°C, a result opposite to the present case of $La_{0.5}Ce_{0.5}FeO_3$ (Fig. 8a). In the case of $La_{0.6}Sr_{0.4}CoO_3$, a relatively sharp and intense peak ($T_M$=820°C, β-state) was evident, a behavior not seen in the present solids. Large amounts of $O_2$ desorption were measured [56], a result also obtained in the present work (see Table 2).

For the present $La_{1-x-y}Sr_xCe_yFeO_3$ materials, desorption of $O_2$ starts at higher temperatures and the TPD profiles are more complex as compared to the above referenced perovskite-type solids [53–56]. Deconvolution of the TPD response resulted in four peaks desorbing in the temperature range 250–750°C (Fig. 8d). These adsorption states could be parallel to the α states described in the previous paragraphs. The explanations that are offered concerning the α states of oxygen adsorption are similar to the ones presented previously for the $La_{1-x}Sr_xMO_{3+\delta}$ (M=Co, Fe, Mn) solids [53,54]. The partial or total substitution of $Ce^{4+}$ by $Sr^{2+}$ leads to the formation of positive holes and/or oxygen vacancies. In addition, partial oxidation of Fe from 3+ to 5+ occurs upon Sr addition as evidenced by Mössbauer studies [38]. The α states of oxygen are therefore ascribed to various adsorbed oxygen species ($O^{n-}$) initially present at various kinds of oxygen vacancies (different coordination environment). McCarty and Wise [57] reported a peak at 627°C for $Fe_2O_3$. The present fourth α-state $O_2$ TPD peak ($T_M$=640°C) does not seem to correspond to the $Fe_2O_3$ phase since it is not observed on the $La_{0.5}Ce_{0.5}FeO_3$ sample which contains a larger amount of $Fe_2O_3$ phase than the rest of the samples.

In the present work, the high temperature β desorption state was also observed but not as a sharp desorption peak. The deconvolution of the TPD response (Fig. 8d) resulted in a high temperature peak centered at around 750°C and desorbing in the range 350–950°C. The amount of this peak largely increases with Sr content in the solid, a result similar to the one observed over the $La_{1-x}Sr_xMO_{3+\delta}$ (M=Co, Fe, Mn) solids but different than the $La_{0.2}Sr_{0.8}Co_{1-y}Fe_yO_3$ ones. The sharp β-state TPD peak was assigned to

reduction of some of the $Co^{3+}$ to $Co^{2+}$, a process not favored in the mixed B-site compositions, where the $Co^{3+}$ ions are stabilized by the presence of Fe ions. The present high-temperature large desorption peak (β-state) is rather due to oxygen diffusion from the bulk to the crystal surface with a high activation energy barrier to be compared with the other four α states of $O_2$ desorption due mainly to surface lattice oxygen. The large amount of oxygen absorbed in the β-state may also suggest the presence of cationic defects (positive holes) within the $SrFeO_{3-x}$ phase. It might be unlikely that this phase could accommodate interstitially in its lattice such large amounts of oxygen. It could, therefore, be suggested that the β-state of oxygen must be ascribed to oxygen species initially present at defect positions (oxygen vacancy/positive hole) in the $SrFeO_{3-x}$ crystal lattice.

### 4.5. Oscillatory behavior during $O_2$ TPD

Numerous reports have appeared in the literature dealing with observed oscillatory behavior in heterogeneous catalytic reaction systems and their interpretation based on different mechanisms and mathematical modeling. A recent review by Schüth et al. [58] gives an excellent overview of the phenomenon. On the other hand, there is no report, to our knowledge, on an oscillatory behavior during temperature programmed desorption studies of a single adsorbed species from a catalytic surface. In the present work, an oscillatory behavior during thermal desorption of $O_2$ has been observed from the surface of $La_{0.5}Sr_{0.2}Ce_{0.3}FeO_3$ (Fig. 8b) and $La_{0.5}Sr_{0.5}FeO_3$ (Fig. 8d) solids but not from the surface of the other two mixed oxidic/perovskitic materials investigated. Based on the accumulated knowledge on the possible mechanisms that can account for oscillations in the rate of a heterogeneous catalytic reaction system, the following discussion is offered that explains in a satisfactory manner the observed oscillations.

It is known that in the structure of $ABO_{3-x}$ perovskite, the oxygen atom is coordinated in different ways as illustrated in Scheme 1 [31]. Based on this scheme, the binding energy of oxygen in each of the clusters shown is different. It is also known that for the oxygen to desorb two adjacent such clusters must exist on the surface (bimolecular desorption kinetics). The mechanism by which the surface oxygen vacancies corresponding to the oxygen sites shown in the clusters of Scheme 1 are filled, before desorption takes place, is that of bulk diffusion.

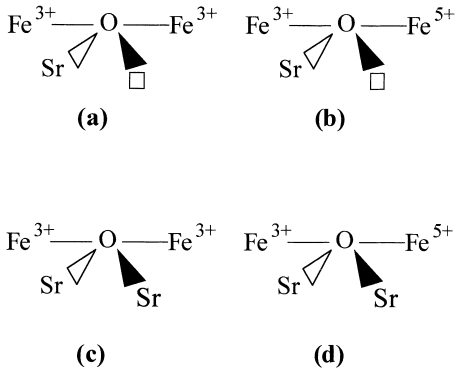


Scheme 1. Different kinds of coordinated oxygen species on the surface of $SrFeO_{3-x}$ perovskite-type material.

Let us consider the fact that desorption of oxygen takes place (a) via recombination of two oxygen atoms from a large pool of one kind of surface lattice oxygen, and (b) via recombination of an oxygen atom from the latter pool with an oxygen atom from a small pool of a second kind of surface lattice oxygen. These two kinds of surface oxygen pools are filled during TPD via bulk oxygen diffusion but with different rates. In particular, the rate of diffusion of bulk oxygen towards the small pool of surface oxygen vacancies is significantly lower than the other one. A normal TPD response (no oscillations) would be that due only to desorption of $O_2$ from the large pool. However, based on what is mentioned above, at a given temperature during this transient process, a higher oxygen desorption rate could develop due to the contribution of the second kind of surface oxygen species. If the rate of depletion of this small pool of oxygen species by desorption is higher than that of filling by bulk diffusion, then suddenly the rate of $O_2$ desorption drops to a lower value. An oscillatory behavior then develops with increasing temperature, the amplitude and the period of which will depend on the relative rates of bulk oxygen diffusion towards the two kinds of surface oxygen vacant sites and the kinetics of $O_2$ desorption from these sites. The concept of having a buffer kinetic step in the series of elementary steps of a reaction in order to produce an oscillatory behavior has been extensively used by many investigators [58]. At present, other mechanisms

that could explain the observed TPD of $O_2$ oscillations are not excluded.

## 5. Conclusions

The following conclusions can be derived from the results of the present work:

- The $La_{0.5}Sr_xCe_yFeO_3$ solids consist of various kinds of crystal phases with $LaFeO_3$, $SrFeO_{3-x}$, $\alpha$-$Fe_2O_3$ and $CeO_2$ being the main ones. Mössbauer studies (at 20 K) revealed that on the samples containing the $SrFeO_{3-x}$ phase, a $Fe^{+3}$ to $Fe^{+5}$ charge disproportionation occurs.
- The catalysts containing both Sr and Ce perform better for the NO+CO reaction as compared to the catalysts containing only Sr or Ce based on the observed conversion of NO or the reaction rate per gram of solid. However, based on the TOF values calculated (site reactivity, $s^{-1}$), the $La_{0.5}Ce_{0.5}FeO_3$ solid has the highest TOF value at 300°C as compared to the other three tested catalysts. In view of these results, an increased surface area of $La_{0.5}Ce_{0.5}FeO_3$ solid is expected to result in higher NO conversions and integral reaction rates.
- The catalysts containing Sr were found to be the best for the NO+$CH_4$+$O_2$ reaction. The $La_{0.5}Sr_{0.2}Ce_{0.3}FeO_3$ solid at $T$=400°C possesses both the highest TOF value and the highest reaction rate compared to the other catalysts.
- The comparison of the activity between $La_{0.5}Sr_x$-$Ce_yFeO_3$ and a wide variety of catalysts from the literature for both reactions, NO+CO and NO+$CH_4$+$O_2$, is very encouraging. Regardless of the low specific surface area of La–Sr–Ce–Fe–O materials, they exhibit one of the highest activities with reference to other perovskite-type catalysts. More importantly, their activity for the NO+CO reaction, in terms of TOF, is found to be comparable to that of $Rh/Al_2O_3$ catalyst.
- The $La_{0.5}Sr_xCe_yFeO_3$ solids exhibit a monotonic significant increase in their oxygen adsorption uptake with increasing Sr content, while a rather small increase in the NO chemisorption uptake is found. It is concluded that for the present solids, $Sr^{2+}$ largely contributes to the creation of oxygen vacancies and to a lesser extent of cationic vacancies. In addition, the bonding strength of both $O_2$ and NO with the surface of the present solids was found to largely depend on their composition.
- Finally, an oscillatory behavior during TPD studies is reported. The oscillatory behavior observed during $O_2$ TPD experiments on $La_{0.5}Sr_{0.2}Ce_{0.3}FeO_3$ and $La_{0.5}Sr_{0.5}FeO_3$ solids was explained as follows. The rate of oxygen desorption is controlled by both the concentration of depleted lattice oxygen species and a slow step of bulk lattice oxygen diffusion towards a specific kind of a surface oxygen vacancy.

## References

[1] A. Fritz, V. Pitchon, Appl. Catal. B 13 (1997) 1.
[2] V.I. Pârvulescu, P. Grange, B. Delmon, Catal. Today 46 (1998) 233.
[3] R.M. Heck, R.J. Farrauto, Catalytic Air Pollution Control-Commercial Technology, Von Nostrand Reinhold, New York, 1995.
[4] E.S.J. Lox, B.H. Engler, in: G. Ertl, H. Knozinger, J. Weitkarnp (Eds.), Handbook of Heterogeneous Catalysis, Vol. 4, VCH, Weinheim, 1997, p. 1559.
[5] A. Trovarelli, Catal. Rev.-Sci. Eng. 35 (1996) 439.
[6] K. Kato, H. Nohira, K. Nakanishi, S. Iguchi, T. Kihara, H. Muraki, European Patent 0 573 672-A1 (1993).
[7] W. Bögner, M. Krämer, B. Krutzsch, S. Piscinger, D. Voigtländer, G. Wenniger, F. Wirbeleit, M.S. Brogan, R.J. Brisley, D.E. Webster, Appl. Catal. B 7 (1995) 153.
[8] M. Öcal, R. Oukaci, G. Marcelin, S.K. Agarwal, Ind. Eng. Chem. Res. 33 (1994) 2930.
[9] N. Mizuno, M. Tanaka, M. Misono, J. Chem. Soc., Faraday Trans. 88 (1992) 91.
[10] A. Lindstedt, D. Strömberg, M. Abul Milh, Appl. Catal. A 116 (1994) 109.
[11] Y. Teraoka, H. Nii, S. Kagawa, K. Jansson, M. Nygren, J. Mater. Chem. 6 (1996) 97.
[12] V.C. Belessi, P.N. Trikalitis, A.K. Ladavos, T.V. Bakas, P.J. Pomonis, Appl. Catal. A 177 (1999) 53.
[13] A.K. Ladavos, P.J. Pomonis, Appl. Catal. B 1 (1992) 101.
[14] R.J.H. Voorhoeve, J.P. Remeika, L.E. Trimble, in: R.L. Klimisch, J.G. Larson (Eds.), The Catalytic Chemistry of Nitrogen Oxides, Plenum Press, New York, 1975, p. 215.
[15] D. Ferri, L. Forni, A.P. Dekkers, B.E. Nieuwenhuys, Appl. Catal. B 16 (1998) 339.
[16] J.C. Menezo, S. Inkari, T. Bertin, J. Barbier, N. Davias-Bainier, R. Noirot, T. Seguelong, Appl. Catal. B 15 (1998) L1.
[17] S.K. Agarwal, B.W.-L. Jang, R. Oukaci, A. Riley, G. Marcelin, in: J.N. Armor (Ed.), Environmental Catalysis, Chapter 18, ACS Symposium of South American Chemical Society, 1994, p. 224.
[18] T. Kudo, T. Gejo, K. Yoshida, Environ. Sci. Technol. 12 (1978) 185.
[19] N. Guilhaume, M. Primet, J. Catal. 165 (1997) 197.

[20] R.J.H. Voorhoeve, in: J.J. Burton, R.L. Garten (Eds.), Advanced Materials in Catalysis, Academic Press, London, 1977, p. 10.
[21] E. Novák, D. Sprinceana, F. Solymosi, Appl. Catal. A 149 (1997) 89.
[22] S.H. Oh, C.C. Eickel, J. Catal. 128 (1991) 526.
[23] F. Fajardie, J.-F. Tempère, J.-M. Manoli, O. Touret, G. Blanchard, G. Djèga-Mariadassou, J. Catal. 179 (1998) 469, and references therein.
[24] K. Tabata, M. Misono, Catal. Today 8 (1990) 249.
[25] H. Furukawa, T. Harada, Y. Teraoka, S. Kagawa, in: Proceedings of the 68th Meeting of Catalysis Society of Japan (A), 1991, p. 4H215.
[26] T. Seiyama, Catal. Rev.-Sci. Eng. 34 (1992) 281.
[27] A.K. Ladavos, P.J. Pomonis, Appl. Catal. A 165 (1997) 73.
[28] B. Viswanathan, Catal. Rev.-Sci. Eng. 34 (1992) 337.
[29] T. Nakamura, M. Misono, Y. Yoneda, J. Catal. 83 (1983) 151.
[30] K.S. Chan, J. Ma, S. Jaenicke, G.K. Chuah, Appl. Catal. A 107 (1994) 201.
[31] L.G. Tejuca, J.L.G. Fierro, J.M.D. Tascon, Adv. Catal. 36 (1989) 237.
[32] A. Maijanen, L. Niinistö, O. Tolonen, M. Leskela, Eur. J. Solid State Inorg. Chem. 28 (1991) 437.
[33] G. Longworth, in: G.J. Long (Ed.), Moessbauer Spectroscopy Applied to Inorganic Chemistry, Vol. I, Plenum Press, New York, 1984, p. 43.
[34] C.N. Costa, A.M. Efstathiou, J. Catal., submitted for publication.
[35] S.-T. Shen, H.-S. Weng, Ind. Eng. Chem. Res. 37 (1998) 2654.
[36] T. Nitadori, M. Misono, J. Catal. 93 (1985) 459.
[37] S.E. Dann, D.B. Currie, M.T. Weller, J. Solid State Chem. 109 (1994) 134.
[38] V.C. Belessi, T.V. Bakas, P.J. Pomonis, Appl. Catal., submitted for publication.
[39] A. Martínez-Arian, M. Fernández-García, J. Soria, J.C. Conesa, J. Catal. 182 (1999) 367.
[40] S. Shin, H. Arakawa, Y. Hatakeyama, K. Ogawa, K. Shimomura, Mater. Res. Bull. 14 (1979) 633.
[41] J. Bartoň, Collect Czech., Chem. Commun. 55 (1990) 1935.
[42] N. Mizuno, H. Toyama, M. Tanaka, M. Yamato, M. Misono, Bull. Chem. Soc. Jpn. 64 (1991) 1383.
[43] N. Mizuno, Y. Fujiwara, M. Misono, J. Chem. Soc., Chem. Commun. (1989) 316.
[44] N. Mizuno, M. Yamato, M. Tanaka, M. Misono, J. Catal. 132 (1991) 560.
[45] A.D. Cowan, R. Dümpelmann, N.W. Cant, J. Catal. 151 (1995) 356.
[46] Y. Li, J.N. Armor, Appl. Catal. B 3 (1993) L1.
[47] Y. Li, J.N. Armor, J. Catal. 145 (1994) 1.
[48] A.W. Aylor, L.J. Lobree, J.A. Reimer, A.T. Bell, J. Catal. 170 (1997) 390.
[49] M.D. Fokema, J.Y. Ying, Appl. Catal. B 18 (1998) 71.
[50] R. Burch, T.C. Watling, Catal. Lett. 43 (1997) 19.
[51] M.A. Peña, J.M.D. Tascón, L.G. Tejuca, Nouv. J. Chim. 9 (1985) 591.
[52] M.A. Peña, J.M.D. Tascón, J.L.G. Fierro, L.G. Tejuca, J. Colloid Interf. Sci. 119 (1987) 100.
[53] T. Seiyama, N. Yamazoe, K. Eguchi, Ind. Eng. Chem. Prod. Res. Dev. 24 (1985) 19.
[54] N. Yamazoe, Y. Teraoka, T. Seiyama, Chem. Lett. (1981) 1767.
[55] Y. Teraoka, M. Yoshimatsu, N. Yamazoe, T. Seiyama, Chem. Lett. (1985) 893.
[56] H.M. Zhang, Y. Shimizu, Y. Teraoka, N. Miura, N. Yamazoe, J. Catal. 121 (1990) 432.
[57] J.G. McCarty, H. Wise, Catal. Today 8 (1990) 231.
[58] F. Schüth, B.E. Henry, L.D. Schmidt, Adv. Catal. 39 (1993) 51.